Computational Investigation of Fractal-Fractional Nonlinear Viscoelastic Fluids Using Local Radial Basis Function Method

Hijaz Ahmad[1,2,3,*]

[1] Irfan Suat Gunsel Operational Research Institute, Near East University, Nicosia/TRNC, 99138, Turkey

[2] Sustainability Competence Centre, Széchenyi István University, Egyetem tér 1, Gyoőr, H-9026, Hungary

[3] VIZJA University, Okopowa 59, Warsaw, 01-043, Poland

INFORMATION

Keywords:
Walter's-B fluid model
Caputo Fractional derivatives
local radial basis functions
thermal radiation
Joule heating

DOI: 10.23967/j.rimni.2026.10.75697

SCIPEDIA Revista Internacional de Métodos Numéricos para Cálculo y Diseño en Ingeniería

Revista Internacional Métodos numéricos para cálculo y diseño en ingeniería RIMNI

In cooperation with CIMNE

Computational Investigation of Fractal-Fractional Nonlinear Viscoelastic Fluids Using Local Radial Basis Function Method

Hijaz Ahmad[1,2,3,*]

[1]Irfan Suat Gunsel Operational Research Institute, Near East University, Nicosia/TRNC, 99138, Turkey

[2]Sustainability Competence Centre, Széchenyi István University, Egyetem tér 1, Gyoőr, H-9026, Hungary

[3]VIZJA University, Okopowa 59, Warsaw, 01-043, Poland

ABSTRACT

Fractal-fractional derivatives generalize both traditional and fractional differentiation approaches by integrating memory effects with fractal properties. This mathematical framework is especially valuable for describing complex systems in which conventional continuum mechanics becomes inadequate, particularly in scenarios involving porous or discontinuous structures. This research investigates the behavior of a non-linear Walter's-B fluid subjected to time-varying thermal and concentration conditions. Beyond the extended derivative formulation, the analysis incorporates phenomena including first-order chemical reactions, radiative heat transfer, Joule heating, Soret effect, and viscous dissipation. The system is also subjected to a transverse magnetic field with magnitude B_0. The fluid model is initially formulated through traditional constitutive equations and subsequently generalized using a fractal-fractional operator. Solutions to this extended model are computed employing a meshfree numerical approach utilizing localized radial basis functions (LRBF), which eliminates the requirement for structured grids and improves precision when addressing intricate geometries. The computational outcomes, displayed through graphical representations, illustrate how the fractional and fractal parameters influence the rheological characteristics of the Walter's-B fluid. These findings establish that adjusting these parameters enables retrieval of classical, fractional, and fractal formulations as particular instances within this comprehensive mathematical structure.

OPEN ACCESS

Received: 06/11/2025

Accepted: 25/12/2025

Published: 20/03/2026

DOI
10.23967/j.rimni.2026.10.75697

Keywords:
Walter's-B fluid model
Caputo Fractional derivatives
local radial basis functions
thermal radiation
Joule heating

1 Introduction

Non-Newtonian fluids are widely encountered in chemical, biological, and engineering systems, where the linear relationship between stress and strain rate assumed in Newtonian mechanics does not hold. Among the numerous models used to describe non-Newtonian behavior, viscoelastic fluids have attracted considerable attention due to their ability to simultaneously capture viscous and elastic effects. In particular, Walter's-B fluid has been employed extensively to describe materials with complex time-dependent rheological properties, including polymeric solutions, lubricants, and certain

*Correspondence: Hijaz Ahmad (hijaz.ahmad@neu.edu.tr).

biological fluids [1,2]. Traditional continuum approaches, however, are often inadequate for accurately modeling systems involving memory effects, multiscale interactions, or heterogeneous porous media. These limitations necessitate the use of generalized differential operators that extend beyond the scope of integer-order calculus. Fractional calculus has emerged as a powerful tool in this context, providing a mathematical framework for incorporating hereditary and memory-dependent effects in fluid models. Classical fractional derivatives, such as the Caputo and Riemann–Liouville formulations, have been widely applied to non-Newtonian fluid mechanics, heat transfer, and anomalous diffusion problems [3,4]. Nevertheless, many physical processes cannot be adequately described using fractional operators alone, particularly when the medium exhibits inherent fractal geometry or discontinuities. To address these challenges, fractal-fractional derivatives have recently been proposed as an extension of classical fractional frameworks. These operators combine the long-memory effects of fractional calculus with the irregularity of fractal geometries, thereby enabling the modeling of systems that lie beyond the scope of traditional continuum mechanics [5–7]. Such formulations are particularly useful for flows in porous structures, heterogeneous materials, and biological tissues, where both fractal properties and memory effects coexist.

In addition to the generalized differential structure, real-world viscoelastic fluid flows are often influenced by multiple transport and reactive mechanisms. Heat and mass transfer phenomena in non-Newtonian systems can be significantly modified by viscous dissipation, Joule heating, chemical reactions, and thermal radiation [8,9]. The Soret effect, which induces mass flux due to temperature gradients, plays an important role in thermodiffusion processes and is especially relevant in chemical engineering applications [10]. The combined presence of these effects produces intricate coupling between momentum, energy, and species concentration fields, leading to highly nonlinear dynamics. External magnetic fields further enrich the problem by introducing magnetohydrodynamic (MHD) effects, which are crucial for controlling the stability and transport characteristics of electrically conducting fluids [11]. The present study focuses on the interaction of these mechanisms within a fractal-fractional extension of the Walter's-B model.

The application of fractional derivatives to non-Newtonian fluids has been the subject of extensive research in recent years. Early studies utilized Caputo and Riemann–Liouville operators to model viscoelastic behaviors in Oldroyd-B, Maxwell, and Walter's-B fluids, demonstrating that fractional models provide better agreement with experimental observations compared to classical integer-order formulations. These works established the importance of fractional derivatives in capturing memory effects in heat and mass transfer [12,13]. Recently, the notion of fractal-fractional calculus has been introduced as a promising generalization that simultaneously accounts for hereditary memory and fractal geometry. Atangana and co-workers pioneered the use of fractal-fractional operators in fluid flow and diffusion problems, showing that the inclusion of a fractal dimension parameter significantly enriches the model's descriptive capacity [14,15]. Applications in porous media, chaotic systems, and biological tissues have further confirmed the versatility of this framework. In fluid dynamics, fractal-fractional formulations allow recovery of classical, fractional, and fractal models as special cases, thereby unifying multiple modeling paradigms under a single operator [16,17]. Fractional-order control strategies have shown clear advantages in engineering applications; for example, demonstrated improved performance in electrohydraulic systems using a fractional PID controller, while Yin et al. reported enhanced robustness and vibration suppression in active suspension systems through a fractional-order approach [18,19]. Recent studies on active suspension systems illustrate the broad interest in advanced control strategies for improving vehicle ride comfort and dynamics, including fractional-order PID control for active suspension positioning and wave-based control methodologies [20,21]. The work reported in [22] focuses on the derivation of exact soliton solutions

and the investigation of dynamical behaviors of the nonlinear Schrödinger equation formulated with Atangana's conformable fractional derivative. By employing analytical techniques alongside phase–plane analysis, the authors uncover a variety of complex wave structures and bifurcation phenomena. In a related contribution, Alam et al. [23] present a comprehensive bifurcation analysis and solitary wave study of a fractional nonlinear soliton neuron model. Their approach combines the modified (G'/G)-expansion method with Jumarie's fractional derivative, leading to explicit analytical solutions and deeper insight into the underlying nonlinear dynamics.

The Walter's-B fluid model, first proposed for describing non-linear viscoelastic effects, has been widely applied to magnetohydrodynamic flows, heat transfer in channels, and oscillatory problems [24,25]. Studies incorporating thermal radiation, Joule heating, and chemical reactions into Walter's-B fluids with fractional operators have provided insights into the influence of fractional parameters on flow and transport phenomena. However, these contributions are largely limited to classical fractional models, while the impact of fractal-fractional derivatives on nonlinear Walter's-B fluids remains underexplored. To the best of our knowledge, systematic computational investigations combining fractal-fractional operators with nonlinear viscoelastic fluids have not yet been reported. From a computational perspective, solving nonlinear fractal-fractional models presents substantial challenges. Traditional numerical methods such as finite difference and finite element techniques often require structured meshes and may suffer from reduced efficiency in complex geometries. To overcome these limitations, meshless methods based on radial basis functions (RBFs) have been developed and widely applied in engineering and applied mathematics [26,27]. Among these, the local radial basis function (LRBF) approach provides an efficient framework for approximating solutions of partial differential equations without requiring domain meshing. LRBF methods are particularly well-suited for fractal-fractional operators, as they combine high flexibility with accuracy in handling irregular domains and non-local operators. Recent works have demonstrated the effectiveness of RBF-based methods in fractional and fractal-fractional problems, though applications to viscoelastic fluid dynamics remain relatively scarce [28,29].

The present work formulates and solves a generalized nonlinear Walter's-B fluid model with fractal-fractional derivatives. The governing equations are extended to incorporate viscous dissipation, chemical reactions, Joule heating, thermal radiation, and Soret effects, under the influence of a transverse magnetic field. Numerical solutions are obtained using the LRBF method, which circumvents the difficulties associated with structured meshing and enhances solution accuracy. Graphical results are presented to highlight the impact of fractional and fractal parameters on the velocity, temperature, and concentration fields. The findings demonstrate that the proposed formulation not only recovers classical and fractional models as limiting cases but also provides new insights into the role of fractal-fractional operators in nonlinear viscoelastic fluid flows.

2 Mathematical Modeling

This study examines an unsteady non-linear Walter's-B fluid confined within a vertical channel, accounting for phenomena including viscous dissipation, chemical reaction, Joule heating, and Soret effects. A uniform transverse magnetic field of magnitude B_0 is applied to the right plate. The system initially remains quiescent under ambient concentration and temperature conditions. For $\bar{\tau} > 0$, the right plate undergoes sinusoidal oscillations, generating disturbances that propagate through the fluid and induce motion. Concurrently, the fluid's temperature and concentration profiles evolve according to $\phi_\infty + (\phi_w - \phi_\infty)\, B\tilde{\tau}$ and $\psi_\infty + (\psi_w - \psi_\infty)\, B\bar{\tau}$, respectively. The geometric configuration of this flow system is depicted in Fig. 1, while Table 1 presents the nomenclature used in this study.

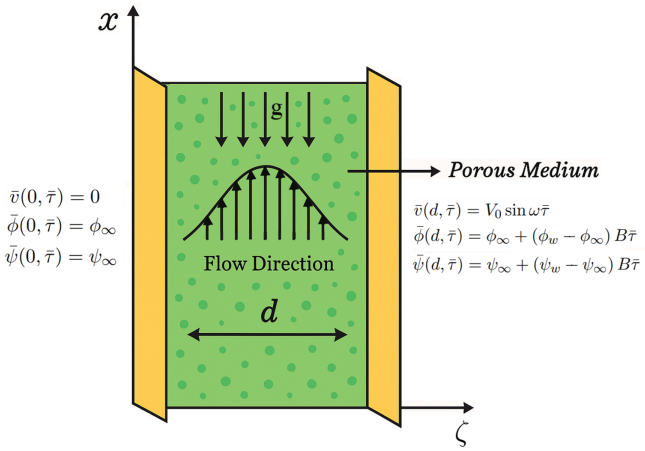

Figure 1: Illustrative diagram of the fluid motion

Table 1: An overview of the nomenclature used

Symbol	Name	Symbol	Name
α	Fractional order	λ_0	Chemical reaction parameter
β	Fractal dimension	S_r	Soret number
υ	Fluid velocity	G_r	Thermal Grashof number
phi	Fluid temperature	S_c	Schmidth number
psi	Fluid concentration	E_C	Eckert number
P_r	Prandtl number	J_h	Joule heating parameter
Rd	Radiation parameter	$\hbar$	Walter's-B fluid parameter
λ	Magnetic number	G_m	Mass Grashof number

The nonlinear Walter's-B fluid model is characterized by the governing equations presented below [30].

$$\frac{\partial \bar{v}(\bar{\zeta},\bar{\tau})}{\partial \bar{\tau}} = v\frac{\partial^2 \bar{v}(\bar{\zeta},\bar{\tau})}{\partial \bar{\zeta}^2} - \frac{k_0}{\rho}\frac{\partial^3 \bar{v}(\bar{\zeta},\bar{\tau})}{\partial \bar{\tau}\partial \bar{\zeta}^2} - \frac{\sigma B_0^2}{\rho}\bar{v}(\bar{\zeta},\bar{\tau}) + g\beta_\phi\left(\bar{\phi}(\bar{\zeta},\bar{\tau}) - \phi_\infty\right) + g\beta_\psi\left(\bar{\psi}(\bar{\zeta},\bar{\tau}) - \psi_\infty\right), \tag{1}$$

$$\rho C_p \frac{\partial \bar{\phi}(\bar{\zeta},\bar{\tau})}{\partial \bar{\tau}} = k\frac{\partial^2 \bar{\phi}(\bar{\zeta},\bar{\tau})}{\partial \bar{\zeta}^2} + \frac{\sigma \tilde{B}_0^2}{\rho}\bar{v}^2(\bar{\zeta},\bar{\tau}) + \mu\left(\frac{\partial \bar{v}(\bar{\zeta},\bar{\tau})}{\partial \bar{\zeta}}\right)^2 - \frac{\partial \tilde{q}_r}{\partial \bar{\zeta}}, \tag{2}$$

$$\frac{\partial \bar{\psi}(\bar{\zeta},\bar{\tau})}{\partial \bar{\tau}} = D\frac{\partial^2 \bar{\psi}(\bar{\zeta},\bar{\tau})}{\partial \bar{\zeta}^2} + \frac{DK_\phi}{\phi_m}\frac{\partial^2 \bar{\phi}(\bar{\zeta},\bar{\tau})}{\partial \bar{\zeta}^2} - K_r\left(\bar{\psi}(\bar{\zeta},\bar{\tau}) - \psi_\infty\right). \tag{3}$$

Here, $\tilde{q}_r = -\frac{4\omega_0}{3\beta_0}\frac{\partial\bar{\phi}}{\partial\bar{\zeta}}$ and the initial and boundary conditions are

$$\left.\begin{aligned}
&\bar{v}(\bar{\zeta},0)=0, \quad \bar{\phi}(\bar{\zeta},0)=\phi_\infty, \quad \bar{\psi}(\bar{\zeta},0)=\psi_\infty,\\
&\bar{v}(0,\bar{\tau})=0, \quad \bar{\phi}(0,\bar{\tau})=\phi_\infty, \quad \bar{\psi}(0,\bar{\tau})=\psi_\infty,\\
&\bar{v}(d,\bar{\tau})=V_0\sin\omega\bar{\tau}, \quad \bar{\phi}(d,\bar{\tau})=\phi_\infty+(\phi_w+\phi_\infty)\,B\bar{\tau}, \quad \bar{\psi}(d,\bar{\tau})=\psi_\infty+(\psi_w+\psi_\infty)\,B\bar{\tau}.
\end{aligned}\right\}$$

Introducing the following dimensionless entities

$$\upsilon=\frac{\bar{v}}{V_0},\tau=\frac{\nu}{d^2}\bar{\tau},\zeta=\frac{\bar{\zeta}}{d},\phi=\frac{\bar{\phi}-\phi_\infty}{\phi_w-\phi_\infty},\psi=\frac{\bar{\psi}-\psi_\infty}{\psi_w-\psi_\infty}. \tag{4}$$

By substituting the quantities defined in Eq. (4) into Eqs. (1)–(3), we obtain the following form:

$$\frac{\partial\upsilon(\zeta,\tau)}{\partial\tau}=\frac{\partial^2\upsilon(\zeta,\tau)}{\partial\zeta^2}-\hbar\left(\frac{\partial^3\upsilon(\zeta,\tau)}{\partial\tau\partial\zeta^2}\right)-\lambda\upsilon(\zeta,\tau)+G_r\phi(\zeta,\tau)+G_m\psi(\zeta,\tau) \tag{5}$$

$$\frac{\partial\phi(\zeta,\tau)}{\partial\tau}=P_r\frac{\partial^2\phi(\zeta,\tau)}{\partial\zeta^2}+J_h\upsilon^2(\zeta,\tau)+E_c\left(\frac{\partial\upsilon(\zeta,\tau)}{\partial\zeta}\right)^2 \tag{6}$$

$$\frac{\partial\psi(\zeta,\tau)}{\partial\tau}=\frac{1}{Sc}\frac{\partial^2\psi(\zeta,\tau)}{\partial\zeta^2}+S_r\frac{\partial^2\phi(\zeta,\tau)}{\partial\zeta^2}-\lambda_\circ\psi(\zeta,\tau) \tag{7}$$

along with

$$\begin{aligned}
&\upsilon(\zeta,0)=0,\phi(\zeta,0)=0,\psi(\zeta,0)=0,\\
&\upsilon(0,\tau)=0,\phi(0,\tau)=0,\psi(0,\tau)=0,\\
&\upsilon(1,\tau)=\sin\omega\tau,\phi(1,\tau)=\tau,\psi(1,\tau)=\tau.
\end{aligned} \tag{8}$$

Eqs. (5)–(7), in their generalized fractal–fractional formulation, are written as

$${}^{FF}D_\tau^{\alpha,\beta}\upsilon(\zeta,\tau)=\frac{\partial^2\upsilon(\zeta,\tau)}{\partial\zeta^2}-\hbar\left(\frac{\partial^3\upsilon(\zeta,\tau)}{\partial\tau\partial\zeta^2}\right)-\lambda\upsilon(\zeta,\tau)+G_r\phi(\zeta,\tau)+G_m\psi(\zeta,\tau) \tag{9}$$

$${}^{FF}D_\tau^{\alpha,\beta}\phi(\zeta,\tau)=P_r\frac{\partial^2\phi(\zeta,\tau)}{\partial\zeta^2}+J_h\upsilon^2(\zeta,\tau)+E_c\left(\frac{\partial\upsilon(\zeta,\tau)}{\partial\zeta}\right)^2 \tag{10}$$

$${}^{FF}D_\tau^{\alpha,\beta}\psi(\zeta,\tau)=\frac{1}{Sc}\frac{\partial^2\psi(\zeta,\tau)}{\partial\zeta^2}+S_r\frac{\partial^2\phi(\zeta,\tau)}{\partial\zeta^2}-\lambda_\circ\psi(\zeta,\tau) \tag{11}$$

Upon incorporating the initial condition defined in Eq. (8), we arrive at

$${}^{F}D_\tau^{\alpha}\upsilon(\zeta,\tau)=\beta\tau^{\beta-1}\left\{\frac{\partial^2\upsilon(\zeta,\tau)}{\partial\zeta^2}-\hbar\left(\frac{\partial^3\upsilon(\zeta,\tau)}{\partial\tau\partial\zeta^2}\right)-\lambda\upsilon(\zeta,\tau)+G_r\phi(\zeta,\tau)+G_m\psi(\zeta,\tau)\right\} \tag{12}$$

$${}^{F}D_\tau^{\alpha}\phi(\zeta,\tau)=\beta\tau^{\beta-1}\left\{P_r\frac{\partial^2\phi(\zeta,\tau)}{\partial\zeta^2}+J_h\upsilon^2(\zeta,\tau)+E_c\left(\frac{\partial\upsilon(\zeta,\tau)}{\partial\zeta}\right)^2\right\} \tag{13}$$

$${}^{F}D_\tau^{\alpha}\psi(\zeta,\tau)=\beta\tau^{\beta-1}\left\{\frac{1}{Sc}\frac{\partial^2\psi(\zeta,\tau)}{\partial\zeta^2}+S_r\frac{\partial^2\phi(\zeta,\tau)}{\partial\zeta^2}-\lambda_\circ\psi(\zeta,\tau)\right\}. \tag{14}$$

3 Computational Methodology

3.1 Time Discretization

The Caputo fractional time derivative $\frac{\partial^\alpha \upsilon(\zeta,\tau)}{\partial \tau^\alpha}$ for $\alpha \in (0,1)$ is discretized as follows [31,32]:

$$\frac{\partial^\alpha \upsilon(\zeta,\tau)}{\partial \tau^\alpha} = \begin{cases} \dfrac{1}{\Gamma(1-\alpha)} \int_0^\tau \dfrac{\partial \upsilon(\zeta,\vartheta)}{\partial \vartheta} (\tau-\vartheta)^{-\alpha} d\vartheta, & 0<\alpha<1 \\ \dfrac{\partial \upsilon(\zeta,\tau)}{\partial \tau}, & \alpha = 1. \end{cases} \tag{15}$$

After approximating the first-order derivative in the time-fractional term using a finite difference technique, we get the following:

$$\frac{\partial^\alpha \upsilon(\zeta,\tau_{q+1})}{\partial \tau^\alpha} = \begin{cases} \dfrac{\Delta\tau^{-\alpha}}{\Gamma(2-\alpha)}(\upsilon^{q+1}-\upsilon^q) + \dfrac{\Delta\tau^{-\alpha}}{\Gamma(2-\alpha)} \sum_{p=1}^{q} (\upsilon^{q+1-p}-\upsilon^{q-p})[(p+1)^{1-\alpha}-p^{1-\alpha}] + R^{p+1}(\bar{\mathbf{z}}), & q \geq 1 \\ \dfrac{\Delta\tau^{-\alpha}}{\Gamma(2-\alpha)}(\upsilon^1-\upsilon^0), & q = 0. \end{cases} \tag{16}$$

Considering $A_0 = \dfrac{\Delta\tau^{-\alpha}}{\Gamma(2-\alpha)}$, $p = 0,1,\ldots,q$, and $b_p = (p+1)^{1-\alpha} - p^{1-\alpha}$. The equation above can be expressed as

$$\frac{\partial^\alpha \upsilon(\zeta,\tau_{q+1})}{\partial \tau^\alpha} = \begin{cases} A_0(\upsilon^{q+1}-\upsilon^q) + A_0 \sum_{p=1}^{q} b_p(\upsilon^{q+1-p}-\upsilon^{q-p}) + R^{p+1}(\zeta), & q \geq 1 \\ A_0(\upsilon^1-\upsilon^0), & q = 0. \end{cases} \tag{17}$$

3.2 Numerical Formulation Using the LRBF Method

In this work, the local radial basis function (LRBF) method [33,34] is applied to the governing equations. In the local formulation, the derivatives of $\upsilon(\zeta,\tau)$ at a center point ζ_j are approximated using the function values at a small set of neighbouring nodes, denoted as $\{\zeta_{j_1},\zeta_{j_2},\zeta_{j_3},\ldots,\zeta_{j_{n_j}}\} \subset \{\zeta_1,\zeta_2,\ldots,\zeta_{N^n}\}$, where $n_j \ll N^n$ and $n = 1$. For each center ζ_j, with $j = 1,2,\ldots,N^n$, a local stencil is constructed to carry out the approximation.

$$\upsilon^{(m)}(\zeta_j) \approx \sum_{k=1}^{n_j} \lambda_k^{(m)} \upsilon(\zeta_{j_k}),\ j = 1,2,\ldots,N^n. \tag{18}$$

By substituting the RBF $\varpi(\|\zeta-\zeta_l\|)$ into Eq. (18), the corresponding coefficients $\lambda_k^{(m)}$ are evaluated as follows:

$$\varpi^{(m)}(\|\zeta_j-\zeta_l\|) = \sum_{k=1}^{n_j} \lambda_{j_k}^{(m)} \varpi(\|\zeta_{j_k}-\zeta_l\|),\ l = j_1,j_2,\ldots,j_{n_j}. \tag{19}$$

By rearranging, Eq. (19) takes the following matrix form;

$$\begin{bmatrix} \varpi_{j_1}^{(m)}(\zeta_j) \\ \varpi_{j_2}^{(m)}(\zeta_j) \\ \vdots \\ \varpi_{j_{n_j}}^{(m)}(\zeta_j) \end{bmatrix} = \begin{bmatrix} \varpi_{j_1}^{(m)}(\zeta_{j_1}) & \varpi_{j_2}^{(m)}(\zeta_{j_1}) & \cdots & \varpi_{j_{n_j}}^{(m)}(\zeta_{j_1}) \\ \varpi_{j_1}^{(m)}(\zeta_{j_2}) & \varpi_{j_2}^{(m)}(\zeta_{j_2}) & \cdots & \varpi_{j_{n_j}}^{(m)}(\zeta_{j_2}) \\ \vdots & \vdots & \ddots & \vdots \\ \varpi_{j_1}^{(m)}(\zeta_{j_{n_j}}) & \varpi_{j_2}^{(m)}(\zeta_{j_{n_j}}) & \cdots & \varpi_{j_{n_j}}^{(m)}(\zeta_{j_{n_j}}) \end{bmatrix} \begin{bmatrix} \lambda_{j_1}^{(m)} \\ \lambda_{j_2}^{(m)} \\ \vdots \\ \lambda_{j_{n_j}}^{(m)} \end{bmatrix}, \tag{20}$$

where

$$\varpi_l(\zeta_k) = \varpi(\|\zeta_k - \zeta_l\|), \sim l = j_1, j_2, \ldots, j_{n_j}, \tag{21}$$

for each $k = j_1, j_2, \ldots, j_{n_j}$.

When expressed in matrix form, the above equation becomes:

$$\mathcal{W}_{n_j}^{(m)} = \mathbf{A}_{n_j} \boldsymbol{\lambda}_{n_j}^{(m)}, \tag{22}$$

where

$$\mathcal{W}_{n_j}^{(m)} = \begin{bmatrix} \varpi_{j_1}^{(m)}(\zeta_j) & \varpi_{j_2}^{(m)}(\zeta_j) & \cdots & \varpi_{j_{n_j}}^{(m)}(\zeta_j) \end{bmatrix}^T \tag{23}$$

$$\mathbf{A}_{n_j} = \begin{bmatrix} \varpi_{j_1}^{(m)}(\zeta_{j_1}) & \varpi_{j_2}^{(m)}(\zeta_{j_1}) & \cdots & \varpi_{j_{n_j}}^{(m)}(\zeta_{j_1}) \\ \varpi_{j_1}^{(m)}(\zeta_{j_2}) & \varpi_{j_2}^{(m)}(\zeta_{j_2}) & \cdots & \varpi_{j_{n_j}}^{(m)}(\zeta_{j_2}) \\ \vdots & \vdots & \ddots & \vdots \\ \varpi_{j_1}^{(m)}(\zeta_{j_{n_j}}) & \varpi_{j_2}^{(m)}(\zeta_{j_{n_j}}) & \cdots & \varpi_{j_{n_j}}^{(m)}(\zeta_{j_{n_j}}) \end{bmatrix} \tag{24}$$

$$\boldsymbol{\lambda}_{n_j}^{(m)} = \begin{bmatrix} \lambda_{j_1}^{(m)} & \lambda_{j_2}^{(m)} & \cdots & \lambda_{j_{n_j}}^{(m)} \end{bmatrix}^T. \tag{25}$$

From the Eq.(22), we obtain,

$$\boldsymbol{\lambda}_{n_j}^{(m)} = \mathbf{A}_{n_j}^{-1} \mathcal{W}_{n_j}^{(m)}. \tag{26}$$

By substituting Eq. (26) into Eq. (18), we have

$$\upsilon^{(m)}(\zeta_j) = (\boldsymbol{\lambda}_{n_j}^{(m)})^T \mathbf{V}_{n_j}, \tag{27}$$

where

$$\mathbf{V}_{n_j} = \left[\upsilon(\zeta_{j_1}), \upsilon(\zeta_{j_2}), \ldots, \upsilon(\zeta_{j_{n_j}})\right]^T. \tag{28}$$

3.3 θ-Weighted Scheme

By employing the θ-weighted method to approximate the governing model in the time domain via (17), we derive:

$$\frac{\partial^\alpha \upsilon}{\partial \tau^\alpha} \equiv \mathfrak{L}\upsilon, \tag{29}$$

now for $q \geq 1$

$$A_0\upsilon^{(q+1)} - A_0\upsilon^{(q)} + A_0\sum_{p=1}^{q} b_p(\upsilon^{q+1-p} - \upsilon^{q-p}) = \theta\mathfrak{L}\upsilon^{(q+1)} + (1-\theta)\mathfrak{L}\upsilon^{(q)}, \tag{30}$$

we get

$$\upsilon^{(q+1)} = (A_0\mathcal{I} - \theta\mathfrak{L})^{-1}\left((A_0\mathcal{I} + (1-\theta)\mathfrak{L})\upsilon^{(q)} + A_0\sum_{p=1}^{q} b_p(\upsilon^{q+1-p} - \upsilon^{q-p})\right), \tag{31}$$

in the same way, for $q = 0$

$$\upsilon^{(1)} = (A_0\mathcal{I} - \theta\mathfrak{L})^{-1}\left((A_0\mathcal{I} + (1-\theta)\mathfrak{L})\upsilon^{(0)}\right). \tag{32}$$

After applying the LRBFM, (31) and (32) lead to

$$\upsilon^{(q+1)} = (A_0\mathcal{I} - \theta\mathcal{L})^{-1}\left((A_0\mathcal{I} + (1-\theta)\mathcal{L})\upsilon^{(q)} + A_0\sum_{p=1}^{q} b_p(\upsilon^{q+1-p} - \upsilon^{q-p})\right), \tag{33}$$

$$\upsilon^{(1)} = (A_0\mathcal{I} - \theta\mathcal{L})^{-1}\left((A_0\mathcal{I} + (1-\theta)\mathcal{L})\upsilon^{(0)}\right), \tag{34}$$

where $\mathcal{L}$ represents the weight matrix, and $\mathcal{I}$ denotes the identity matrix corresponding to the differential operator $\mathfrak{L}$. For $\theta = 1$, Eqs. (33) and (34) reduce to the fully implicit scheme.

4 Results and Discussion

In this section, we investigate the nonlinear fractal–fractional model of a Walter's-B fluid flowing through an open bounded channel. The analysis incorporates the effects of viscous dissipation, Joule heating, the Soret effect, chemical reactions, and an applied magnetic field. The classical governing equations are generalized using a fractal–fractional operator, and the resulting system is solved numerically using a LRBF method. All numerical computations and implementations of the LRBF scheme are carried out in the MATLAB programming environment. Graphical results are presented to illustrate the influence of key physical parameters on the fluid flow, heat transfer, and mass transport characteristics.

Fig. 2 depicts a comparative analysis of the velocity fields obtained from the fractal–fractional, fractional, fractal, and classical formulations. It is evident that the velocity distribution is significantly affected by the fractal–fractional order. The fractal dimension ($0 \leq d \leq 2$) quantifies the geometric complexity of the velocity profile: $d = 0$ corresponds to a smooth, uniform distribution, whereas $d = 2$ represents a highly irregular, potentially turbulent flow structure. Similarly, the fractional derivative order governs the memory and non-local behavior of the flow. Orders less than unity imply slower decay of disturbances, whereas orders greater than unity accelerate the relaxation. This enriched modeling framework captures memory effects and non-integer scaling, thereby providing a more realistic description of anomalous transport phenomena compared to the classical model.

Fig. 3 depicts the impact of the thermal Grashof number (Gr) on velocity distribution. As Gr increases, buoyancy forces become dominant relative to viscous forces, enhancing the velocity. Physically, higher Gr leads to stronger thermal convection, which destabilizes the flow and intensifies velocity gradients. This phenomenon reflects the onset of natural convection cells in thermally driven flows.

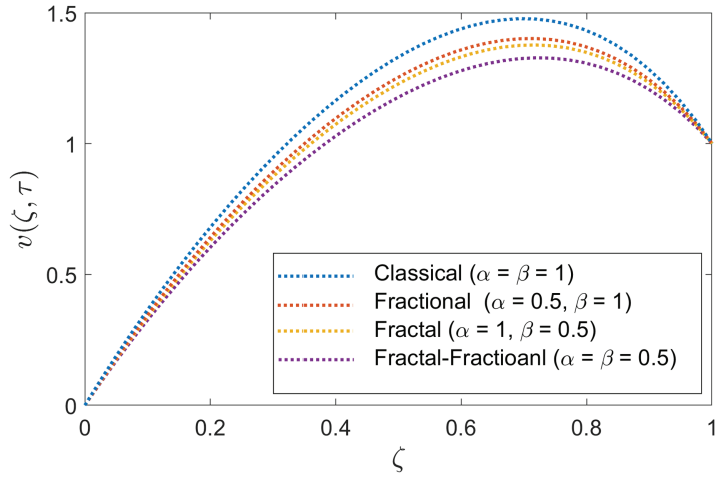

Figure 2: Comparative analysis of fractal-fractional, fractional, fractal, and classical velocity fields

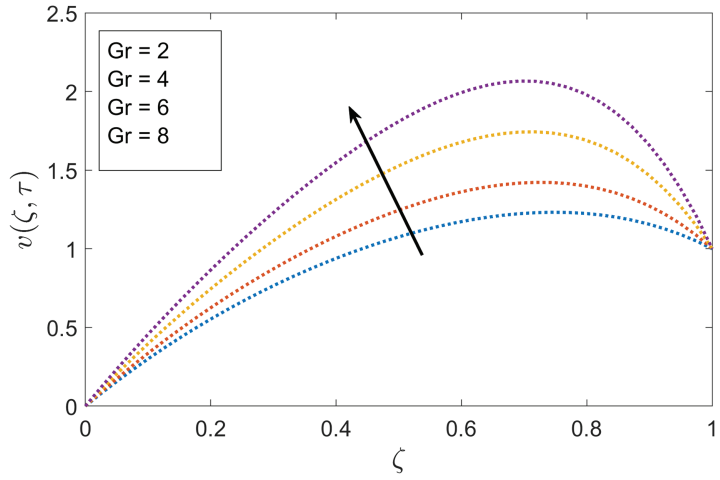

Figure 3: Velocity profile variation with thermal Grashof number *Gr*

Fig. 4 shows the effect of the mass Grashof number (*Gm*). The velocity profile rises with increasing *Gm*, indicating that solutal buoyancy forces play a crucial role in enhancing fluid motion. For small *Gm*, viscous forces dominate, leading to nearly uniform flow, whereas larger *Gm* produces strong buoyancy-driven convection, formation of boundary layers, and eventual transition toward turbulence. Consequently, solutal buoyancy augments mixing and enhances transport processes.

Fig. 5 demonstrates the influence of the magnetic parameter λ. An increase in λ suppresses velocity due to the Lorentz force, which opposes fluid motion and enhances resistive drag. Physically, the magnetic field introduces an additional damping effect, thereby reducing the flow intensity and stabilizing the velocity distribution.

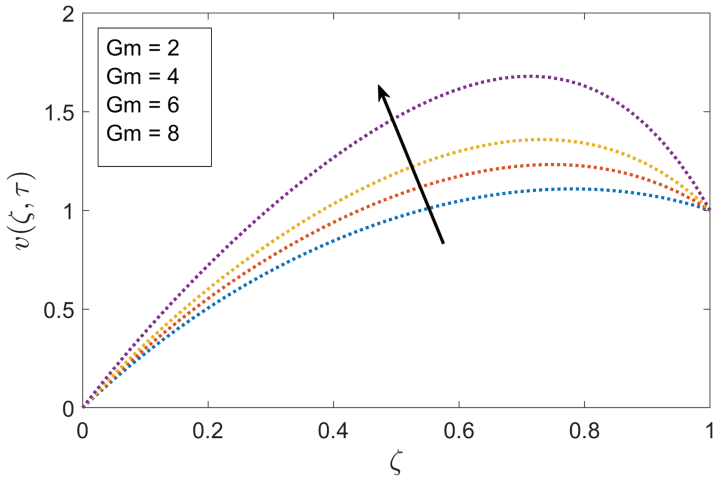

Figure 4: Velocity profile variation with mass Grashof number *Gm*

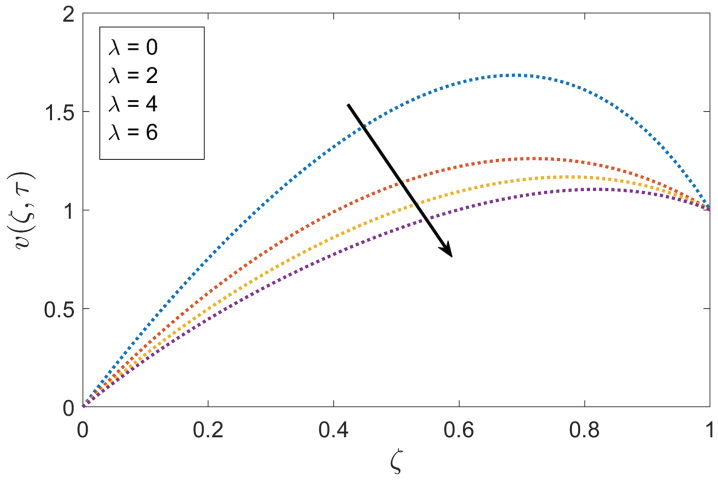

Figure 5: Velocity profile variation with magnetic parameter λ

Fig. 6 highlights the role of the material parameter h of Walter's-B fluid. Increasing h reduces the velocity, as it effectively thickens the momentum boundary layer and retards fluid motion. This outcome is consistent with the viscoelastic nature of Walter's-B fluids.

The impact of the Eckert number (Ec) is illustrated in Fig. 7. Higher values of Ec amplify the thermal field due to the conversion of kinetic energy into internal energy. This leads to elevated fluid temperature and thicker thermal boundary layers.

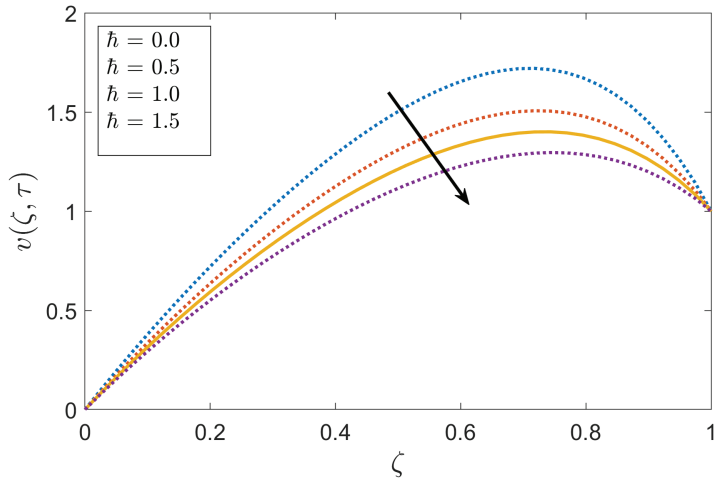

Figure 6: Velocity profile variation with Walter's-B fluid parameter h

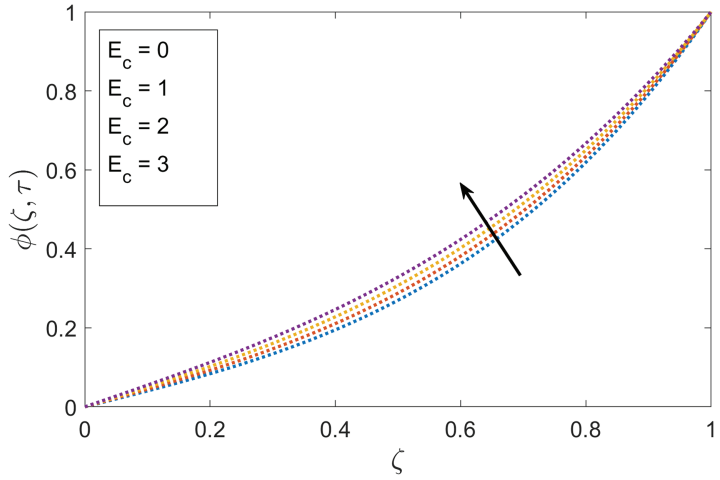

Figure 7: Thermal profile variation with Eckert number Ec

Fig. 8 exhibits the effect of Joule heating parameter Jh. Increasing Jh enhances the thermal field by generating additional resistive heating. This results in larger thermal gradients and elevated temperatures within the flow domain, which may intensify convective transport.

The Prandtl number (Pr) significantly modifies the thermal distribution (Fig. 9). Fluids with high Pr exhibit stronger momentum diffusion relative to thermal diffusion, leading to thinner thermal boundary layers and steeper gradients. Conversely, small Pr enhances thermal diffusion, resulting in broader thermal layers.

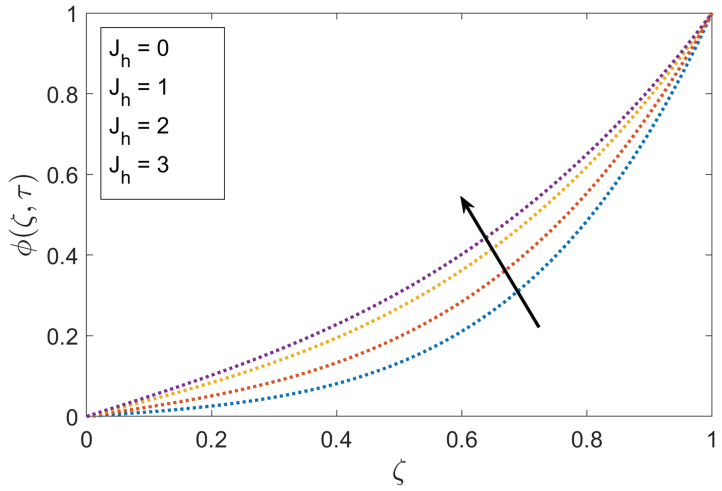

Figure 8: Thermal profile variation with Joule heating parameter *Jh*

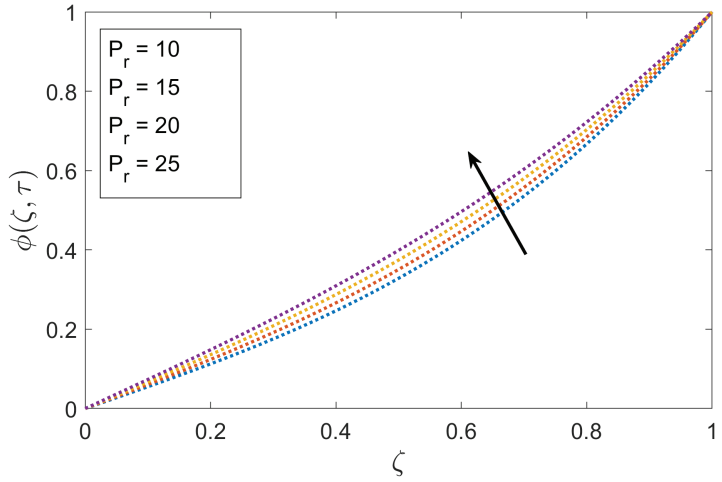

Figure 9: Thermal profile variation with Prandtl number *Pr*

Fig. 10 shows the role of Schmidt number (*Sc*). Larger *Sc* values reduce mass diffusivity, producing steeper concentration gradients near boundaries. Lower *Sc* enhances diffusion, yielding smoother concentration profiles dominated by convective effects.

Fig. 11 displays the influence of the Soret number (*Sr*). In general, a positive *Sr* drives the more diffusive species toward the colder region (thermodiffusion), whereas a negative *Sr* pushes species toward the hotter region (thermophoresis). In this study, the negative *Sr* considered leads to a decreasing concentration profile.

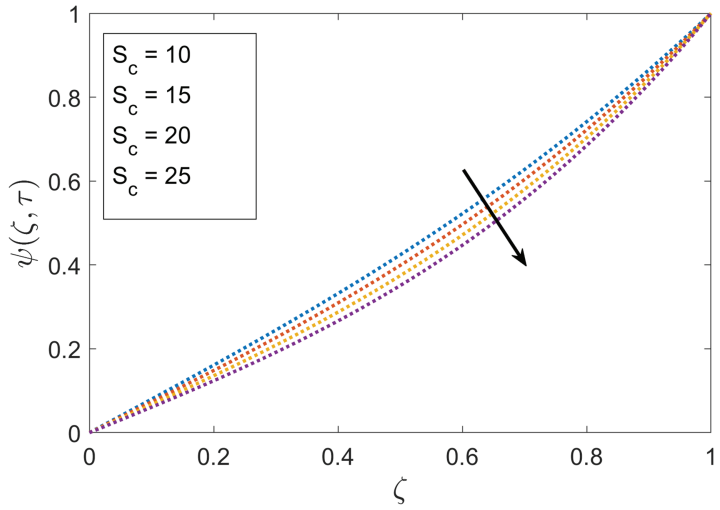

Figure 10: Concentration profile variation with Schmidt number *Sc*

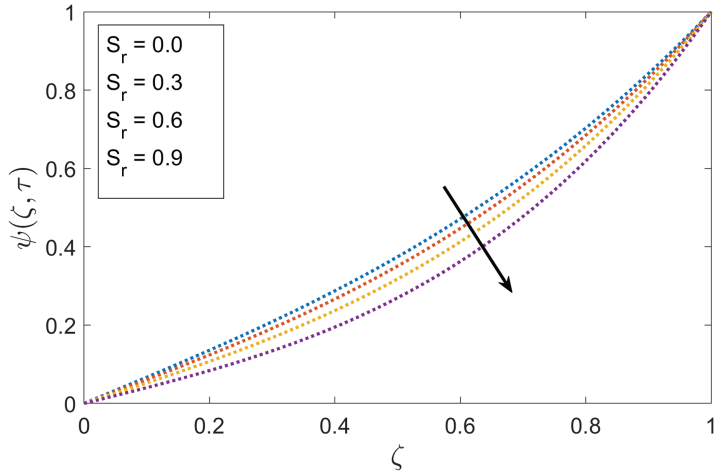

Figure 11: Concentration profile variation with Soret number *Sr*

Finally, Fig. 12 illustrates the impact of the first-order chemical reaction parameter λ_0. An increase in λ_0 reduces concentration levels due to enhanced reactant consumption. The exponential decay in concentration reflects the dominance of reaction kinetics over diffusion at higher reaction rates.

Overall, the results confirm that the fractal-fractional framework effectively captures memory, nonlocality, and anomalous transport effects absent in classical models. This provides deeper insights into the interplay between thermal, solutal, magnetic, and viscoelastic effects in complex fluid systems, with direct applications in engineering and industrial processes.

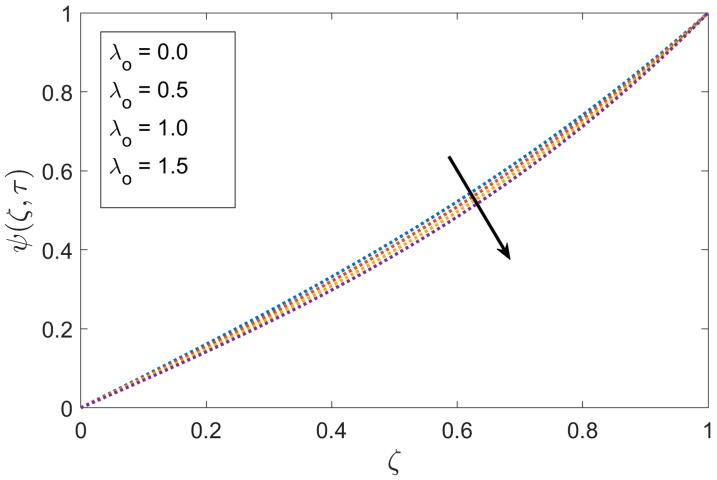

Figure 12: Concentration profile variation with first-order chemical reaction parameter λ_0

5 Conclusion

In this study, a numerical investigation of the nonlinear fractal-fractional model of Walter's-B fluid was carried out under the influences of Joule heating, viscous dissipation, thermal radiation, and the Soret effect. The governing model was generalized by employing the Caputo derivative operator into a fractal-fractional framework, and its numerical findings were obtained using a meshless LRBF method. Graphical representations were generated through computational tools to illustrate the physical behavior of the model.

The key findings can be summarized as follows:

- The fractal-fractional framework demonstrates a significantly stronger memory effect compared to both classical and fractional models. This feature enables the fractal-fractional model to more accurately represent realistic physical phenomena where long-term memory and complexity play a crucial role.
- The velocity field exhibits an increasing trend with respect to the thermal Grashof number (Gr) and mass Grashof number (Gm), whereas it decreases with increasing Walter's-B parameter (h) and magnetic parameter (λ).
- The thermal field decreases with higher Prandtl number (Pr), while it shows an increasing response to Eckert number (Ec), radiation parameter (Rd), and Joule heating parameter (Jh).
- The concentration field decreases with increasing Schmidt number (Sc), while it increases under the influence of the Soret number (Sr).

Overall, the fractal-fractional model provides a more comprehensive and realistic representation of fluid dynamics by incorporating both fractal geometry and memory effects. These findings highlight its potential applications in studying complex transport processes in engineering, physics, and applied sciences.

Acknowledgement: Not applicable.

Funding Statement: The author received no specific funding for this study.

Availability of Data and Materials: Data available on request from the authors. The data that support the findings of this study are available from the corresponding author, upon reasonable request.

Ethics Approval: Not applicable.

Conflicts of Interest: The author declares no conflicts of interest to report regarding the present study.

References

1. Laxmaiah K, Reddy YD. Thermal radiation and chemical reaction effects on MHD Williamson nanofluid flow over an exponentially porous stretching sheet with non-uniform heat source/sink. J Radiat Res Appl Sci. 2025;18(3):101742. doi:10.1016/j.jrras.2025.101742.
2. Ajala OA, Adegbite P. Hydromagnetic flow of micropolar nanofluids with co-effects of thermal radiation and chemical reaction over an inclined permeable stretching surface. Beni-Suef Univ J Basic Appl Sci. 2023;12(1):86. doi:10.1186/s43088-023-00424-2.
3. Podlubny I. Fractional differential equations. Philadelphia, PA, USA: Academic Press; 1999.
4. Hilfer R. Applications of fractional calculus in physics. Singapore: World Scientific; 2000.
5. Kumar D, Baleanu D. Fractional calculus and its applications in physics. Front Phys. 2019;7:81. doi:10.3389/fphy.2019.00081.
6. Elidemir İO, Özarslan MA, Buranay SC. On the analysis of fractional calculus operators with bivariate Mittag Leffler function in the kernel. J Appl Math Comput. 2024;70:1295–323. doi:10.1007/s12190-024-02004-8.
7. Abidin MZ, Marwan M. On the global existence and analyticity of the mild solution for the fractional Porous medium equation. Bound Value Probl. 2023;2023(1):107. doi:10.1186/s13661-023-01794-3.
8. Ali Q, Amir M, Metwally ASM, Younas U, Zubair Jan A, Amjad A. Investigation of MHD fractionalized viscous fluid and thermal memory with slip and Newtonian heating effect: a fractional model based on Mittag-Leffler kernel. J Therm Anal Calorim. 2024;149:8257–70. doi:10.1007/s10973-024-13205-5.
9. Manzoor U, Waqas H, Muhammad T, Wakif A. Oldroyd-B nanofluid flow with the features of bioconvection and Cattaneo-Christov model in the presence of gyrotactic motile microorganism. Waves Random Complex Media. 2022;35(6):10397–419. doi:10.1080/17455030.2022.2112990.
10. Arif U, Nawaz M, Salmi A. Numerical study of simultaneous transport of heat and mass transfer in Maxwell hybrid nanofluid in the presence of Soret and Dufour effects. Phys Scr. 2022;97(2):025207. doi:10.1088/1402-4896/ac4d46.
11. Abbas S, Nisa ZU, Gilani SFF, Nazar M, Metwally ASM, Zubair Jan A. Fractional analysis of magneto-hydrodynamics Maxwell flow over an inclined plate with the effect of thermal radiation. Int J Theor Phys. 2024;63:120. doi:10.1007/s10773-024-05654-3.
12. Giusti A, Colombaro I, Garra R, Garrappa R, Mentrelli A. On variable-order fractional linear viscoelasticity. Fract Calc Appl Anal. 2024;27:1564–78. doi:10.1007/s13540-024-00288-y.
13. Saeed ST, Inc M, Alqarni MZ, Radwan N. Series solution of time-fractional mhd viscoelastic model through non-local kernel approach. Opt Quant Electron. 2024;56:861. doi:10.1007/s11082-024-06674-3.
14. Atangana A, Qureshi S. Modeling attractors of chaotic dynamical systems with fractal-fractional operators. Chaos Solit Fract. 2019;123:320–37. doi:10.1016/j.chaos.2019.04.020.
15. Khan MA, Atangana A. Numerical methods for fractal-fractional differential equations and engineering: simulations and modeling. Philadelphia, PA, USA: CRC Press; 2023. doi:10.1201/9781003359258.
16. Murtaza S, Ahmad Z, Ali IE, Akhtar Z, Tchier F, Ahmad H, et al. Analysis and numerical simulation of fractal-fractional order non-linear couple stress nanofluid with cadmium telluride nanoparticles. J King Saud Univ-Sci. 2023;35(4):102618. doi:10.1016/j.jksus.2023.102618.

17. Partohaghighi M, Mortezaee M, Akgül A, Hassan AM, Sakar N. Numerical analysis of the fractal-fractional diffusion model of ignition in the combustion process. Alex Eng J. 2024;86:1–8. doi:10.1016/j.aej.2023.11.038.
18. Robles EH, Torres FJ, Balvantín-García AJ, Martínez-Ramírez I, Capilla G, Ramírez-Paredes JP. Fractional calculus applied to the generalized model and control of an electrohydraulic system. Fract Fractio. 2024;8(12):679. doi:10.3390/fractalfract8120679.
19. Yin Z, Cui C, Wang R, Su R, Ma X. Improving vehicle dynamics: a fractional-order $PI^{\lambda}D^{\mu}$ control approach to active suspension systems. Machines. 2025;13(4):271. doi:10.3390/machines13040271.
20. Hu Y, Liu J, Wang Z, Zhang J, Liu J. Research on electric oil-pneumatic active suspension based on fractional-order PID position control. Sensors. 2024;24(5):1644. doi:10.3390/s24051644.
21. Habibi H. Control of active suspension systems based on mechanical wave concepts. Actuators. 2025;14(5):230. doi:10.3390/act14050230.
22. Alam MN, Iqbal M, Hassan M, Fayz-Al-Asad M, Hossain MS, Tunç C. Bifurcation, phase plane analysis and exact soliton solutions in the nonlinear Schrodinger equation with Atangana's conformable derivative. Chaos Solit Fract. 2024;182:114724. doi:10.1016/j.chaos.2024.114724.
23. Alam MN, Akash HS, Saha U, Hasan MS, Parvin MW, Tunç C. Bifurcation analysis and solitary wave analysis of the nonlinear fractional soliton neuron model. Iran J Sci. 2023;47(5):1797–808. doi:10.1007/s40995-023-01555-y.
24. Walters K. Overview of macroscopic viscoelastic flow. In: Viscoelasticity and rheology. Philadelphia, PA, USA: Academic Press; 1985. p. 47–79. doi:10.1016/B978-0-12-454940-1.50008-7.
25. Qayyum S, Hayat T, Shehzad SA, Alsaedi A. Effect of a chemical reaction on magnetohydrodynamic (MHD) stagnation point flow of Walters-B nanofluid with Newtonian heat and mass conditions. Nucl Eng Technol. 2017;49(8):1636–44. doi:10.1016/j.net.2017.07.028.
26. Fasshauer GE. Meshfree approximation methods with MATLAB. Singapore: World Scientific; 2007.
27. Liu GR, Gu YT. Meshfree methods: moving beyond the finite element method. Philadelphia, PA, USA: CRC Press; 2010.
28. Ahmad I, Khan MN, Jan R, Razak NNA. Efficient numerical method for pricing multi-asset options with the time-fractional Black-Scholes model: focus on American and digital options. Math Model Control. 2025;5(2):147–63. doi:10.3934/mmc.2025011.
29. Maatki C, Murtaza S, Khan MN, Alrasheedi NH, Alshammari BM, Kolsi L. Mesh-free modeling and analysis of fractal-fractional thermoelectric fluid flow model with thermal radiation in microchannel systems. J Radiat Res Appl Sci. 2025;18(4):101984. doi:10.1016/j.jrras.2025.101984.
30. Ali F, Saqib M, Khan I, Sheikh NA, Jan SAA. Exact analysis of MHD flow of a Walters'-B fluid over an isothermal oscillating plate embedded in a porous medium. Eur Phys J Plus. 2017;132(2):95. doi:10.1140/epjp/i2017-11404-2.
31. Lin Y, Xu C. Finite difference/spectral approximations for the time-fractional diffusion equation. J Comput Phys. 2007;225(2):1533–52. doi:10.1016/j.jcp.2007.02.001.
32. Khan MN, Ahmad I, Shakeel M, Jan R. Fractional calculus analysis: investigating drinfeld-sokolov-wilson system and harry dym equations via meshless procedures. Math Model Control. 2024;4:86–100. doi:10.3934/mmc.2024008.
33. Shakeel M, Khan MN, Ahmad I. Local meshless collocation scheme for numerical simulation of space fractional PDE. Therm Sci. 2023;27:101–9. doi:10.2298/TSCI23S1101S.
34. Ahmad M, Khan MN, Ahmad I. Local meshless methods for elliptic pdes with multipoint boundary conditions: investigating efficiency and accuracy of various rbfs. Eur Phys J Spec Top. 2025;234:2525–42. doi:10.1140/epjs/s11734-024-01416-8.